Journal of Nuclear Materials 396 (2010) 176–180

Contents lists available at ScienceDirect

Journal of Nuclear Materials

journal homepage: www.elsevier.com/locate/jnucmat

# Carbon film growth and hydrogenic retention of tungsten exposed to carbon-seeded high density deuterium plasmas

G.M. Wright [a,*], R.S. Al [a], E. Alves [b], L.C. Alves [b], N.P. Barradas [b], A.W. Kleyn [a,c], N.J. Lopes Cardozo [a,d], H.J. van der Meiden [a], V. Philipps [e], G.J. van Rooij [a], A.E. Shumack [a], W.A.J. Vijvers [a], J. Westerhout [a], E. Zoethout [a], J. Rapp [a,e]

[a] FOM-Institute for Plasma Physics Rijnhuizen, EURATOM-FOM, A Member of the Trilateral Euregio Cluster, Nieuwegein, The Netherlands
[b] Instituto Tecnológico e Nuclear, Sacavém, Portugal
[c] Leiden Institute for Chemistry, Leiden University, Leiden, The Netherlands
[d] Eindhoven University of Technology, Eindhoven, The Netherlands
[e] Institut für Plasmaphysik, FZ Jülich, Association EURATOM, Jülich, Germany

ARTICLE INFO

*Article history:*
Received 12 August 2009
Accepted 2 November 2009

ABSTRACT

Tungsten (W) targets have been exposed to high density ($n_e \leqslant 4 \times 10^{19}$ m$^{-3}$), low temperature ($T_e \leqslant 3$ eV) $CH_4$-seeded deuterium (D) plasma in Pilot-PSI. The surface temperature of the target was ~1220 K at the center and decreased radially to ~650 K at the edges. Carbon film growth was found to only occur in regions where there was a clear CII emission line, corresponding to regions in the plasma with $T_e \geqslant 2$ eV. The maximum film thickness was ~2.1 μm after a plasma exposure time of 120 s. $^3$He nuclear reaction (NRA) analysis and thermal desorption spectroscopy (TDS) determine that the presence of a thin carbon film dominates the hydrogenic retention properties of the W substrate. Thermal desorption spectroscopy analysis shows retention increasing roughly linearly with incident plasma fluence. NRA measures a C/D ratio of ~0.002 in these films deposited at high surface temperatures.



## 1. Introduction

The tungsten–carbon (W–C) system is of high relevance to ITER since these are the materials used in the current design of the ITER divertor. When dealing with mixed-materials, one has to consider both the physics and the chemistry between the two materials. Of particular concern in this system is the formation of tungsten carbides (i.e. WC, $W_2C$) at elevated temperatures and carbon film growth on the tungsten substrate.

The formation of tungsten carbide has been observed from annealing carbon films on tungsten substrates [1] and from irradiation of tungsten targets at elevated temperatures ($T_W \geqslant 850$ K) with carbon-seeded hydrogenic plasmas [2,3]. The latter of these two mechanisms is possible in the ITER divertor since carbon impurities will be eroded, ionized in the plasma and then redistributed to the first wall. The formation of tungsten carbide layers is known to increase hydrogenic retention [4,5], decrease diffusion rates [6], and decrease surface recombination rates [3] as compared to a pure W surface. Formation of carbon films can dominate the retention properties of the tungsten substrate [2].

This investigation focuses on the formation of carbon films and any associated carbide formation in a high plasma flux (~$10^{24}$ m$^{-2}$ s$^{-1}$) environment and how it impacts the hydrogenic retention of the material. It is critical to examine these processes in a high flux regime since carbon-based components in ITER will be located at the divertor strikepoints; meaning the region of strongest W–C interaction will also be the region of highest plasma flux in ITER.

## 2. Experiment

The plasma exposures of tungsten (W) samples were performed in the linear plasma generator Pilot-PSI [7]. A Thomson scattering system measures plasma parameters ~15 mm in front of the target [8]. Typical operation parameters were central electron densities ($n_e$) and temperatures ($T_e$) of $(4.0 \pm 0.5) \times 10^{19}$ m$^{-3}$ and $3.0 \pm 0.3$ eV respectively (Fig. 1). Both $n_e$ and $T_e$ follow a peaked distribution across the plasma column with an e-folding length of $5.5 \pm 0.5$ mm. Surface temperatures were measured with a multi-wavelength pyrometer that allows for automatic compensation of changing emissivity; an important consideration to maintain consistent temperature measurements for carbon films (high emis-

* Corresponding author. Address: FOM-Institute for Plasma Physics Rijnhuizen, Postbus 1207, 3430 BE Nieuwegein, The Netherlands. Tel.: +31 30 6096830; fax: +31 30 6031204.
*E-mail address:* wright@rijnh.nl (G.M. Wright).

0022-3115/$ - see front matter © 2009 Elsevier B.V. All rights reserved.
doi:10.1016/j.jnucmat.2009.11.002

sivity) being deposited on a tungsten (low emissivity) substrate. Central surface temperatures during the exposure were measured to be 1200 ± 30 K with a reduction to 650 ± 70 K at the edges of the plasma column (Fig. 1c).

The carbon was introduced into the deuterium plasma through a methane puffing ring positioned 150 mm downstream from the plasma source (~350 mm upstream from the target). The carbon content of the plasma was monitored with a high resolution spectrometer from 425–435 nm allowing for observation of CII line (426.8 nm), the CH A-X (Gerö) band (429–431.3 nm), and $H_\gamma$(434.0 nm). It should be noted that in these experiments $CH_4$ was puffed into deuterium plasmas so that any detected deuterium in the analysis originates from the plasma. The spectrometer was focussed at a point ~50 mm in front of the target to eliminate any signal contributions from carbon re-erosion from the target surface.

The W targets used were 20 mm in diameter and 1 mm thick, 99.97 at.% pure tungsten purchased from Plansee Metals. The targets were mechanically attached to a water-cooled copper heat sink with a molybdenum clamping ring and were electrically grounded for the exposures. No special preparation (i.e. polishing, annealing) of the targets was performed before exposure in Pilot-PSI. See Table 1 for exposure conditions and nomenclature for each target.

The deposited carbon films were analyzed by proton microbeam Rutherford backscattering (RBS). The non-Rutherford, enhanced cross section between protons and carbon allow for the deposited carbon to be measured above the strong RBS signal from the high-$Z$ W substrate. X-ray Photoelectric Spectroscopy (XPS) was used to examine post-exposure surface conditions and check for tungsten carbide formation. The deuterium trapping was investigated using D($^3$He, p)$\alpha$ Nuclear Reaction Analysis (NRA) and Thermal Desorption Spectroscopy (TDS).

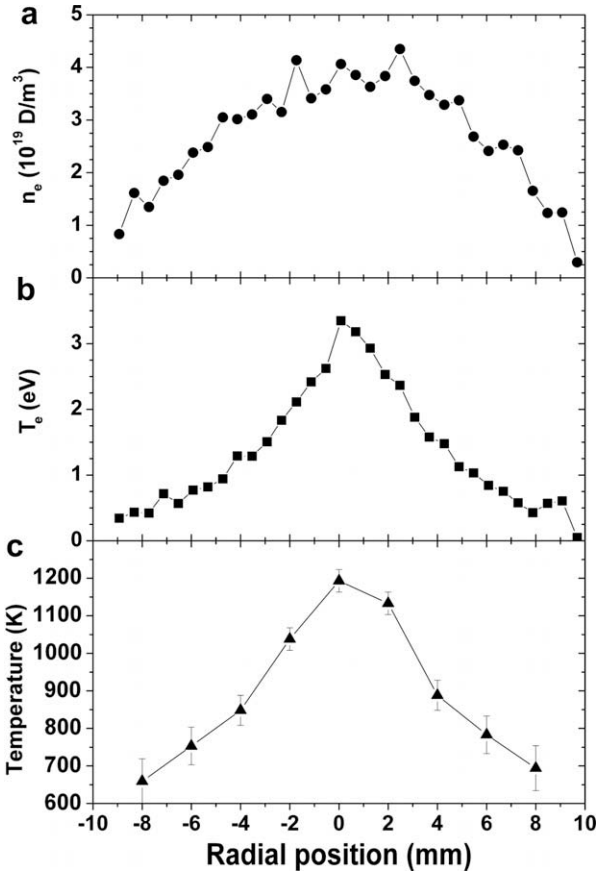


**Fig. 1.** Thomson scattering profiles of (a) electron density, (b) electron temperature taken across the plasma column width and (c) surface temperature measurements for a typical plasma exposure.

## 3. Results and discussion

Optical emission spectroscopy is used to determine the carbon content of the plasma. The peak signal strengths of the CII-line (426.8 nm), CH band (peak at 430.6 nm), and $H_\gamma$ (434.0 nm) are plotted as a function of radial position in Fig. 2 for $CH_4$ flows of 3 sccm (0.003 slm) and 7 sccm (0.007 slm). One can see that both the methane flow rate and plasma parameters (related through the radial position, see Fig. 1a,b) have a strong influence on the carbon content of the deuterium plasma. For a $CH_4$ injection rate of 7 sccm, the CII line is not strong in the outer regions of the plasma but only in the central part of the column with $T_e \geqslant 2$ eV (Fig. 2). For the 3 sccm injection rate, both the CH-band and CII line are strongly reduced as compared to the 7 sccm case, but the $H_\gamma$ remains constant, indicating that the methane puffing is not affecting the hydrogenic content of the plasma. This is not surprising given the low rate of methane puffing (0.003–0.007 slm) compared to the neutral deuterium injection rate into the plasma source (~1.0 slm).

Converting these emission profiles into plasma carbon concentrations is a highly complex process at the low electron temperatures used in this experiment since photon efficiencies no longer follow the standard model [9]. There are experimentally obtained CH photon efficiencies [9] but these are for methane puffing from the surface of the target directly into the plasma column, rather than the puffing ring used to carbon-seed the plasma in this experiment. Nevertheless, since puffing directly into center of the plasma column results in the least amount of injected particles lost before emitting a photon, using these experimentally obtained photon efficiencies provides the *minimum* possible carbon concentrations $((C^+ + C^0)/D^+)$ of 0.003 and 0.0008 for $CH_4$ puff rates of 7 sccm and 3 sccm respectively. To define the *maximum* possible carbon concentration we assume every injected methane atom contributes one carbon atom (or $CH_X$ molecule) to the plasma. Under that assumption a comparison of injected gas rates can yield a maximum carbon concentration. The D gas ($D_2$) is injected into the source at a rate of 1.0 slm. Previous work with the cascaded arc source has shown the ionization efficiency of the source to be ~15% for this gas flow rate [10], meaning an equivalent $D^+$ "gas flow rate" of 0.3 slm. Comparing this with the $CH_4$ injection rates of 0.007 slm and 0.003 slm we obtain *maximum* carbon concentrations of 0.023 and 0.010 respectively. It should be noted that these maximum values are very conservative given we are puffing methane from a ring of diameter 90 mm into a plasma column of diameter < 20 mm. It is likely a significant fraction of the injected gas is pumped out of the system without ever penetrating the plasma which would reduce the *maximum* carbon fraction. However, it can be stated with confidence that the carbon concentrations for plasmas with 7 sccm $CH_4$ injection is in the range 0.003–0.023 and 3 sccm $CH_4$ injection is in the range 0.0008–0.010.

**Table 1**
Carbon seeding conditions and nomenclature for W targets.

| Target | $CH_4$ puff rate | Plasma exposure |
|---|---|---|
| I – 0–120 | 0 sccm | 120 s |
| VI – 7–10 | 7 sccm | 10 s |
| VII – 7–30 | 7 sccm | 30 s |
| IV – 7–60 | 7 sccm | 60 s |
| VIII – 7–120 | 7 sccm | 120 s |
| IX – 3–120 | 3 sccm | 120 s |

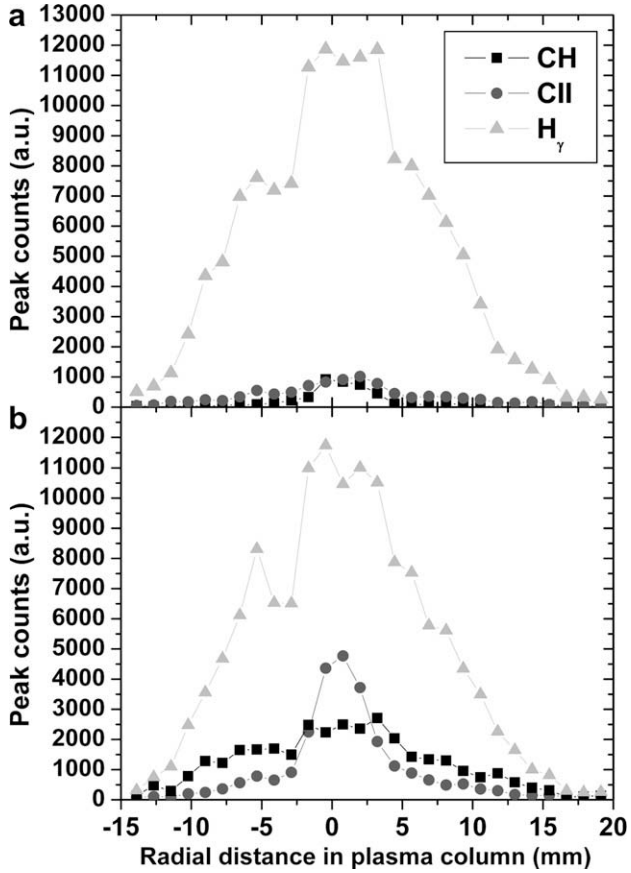


**Fig. 2.** Radial distribution of CII (426.8 nm), CH (430.6 nm) and $H_\gamma$ (434.0 nm) emission signal for methane puffing rates of (a) 3 sccm and (b) 7 sccm.

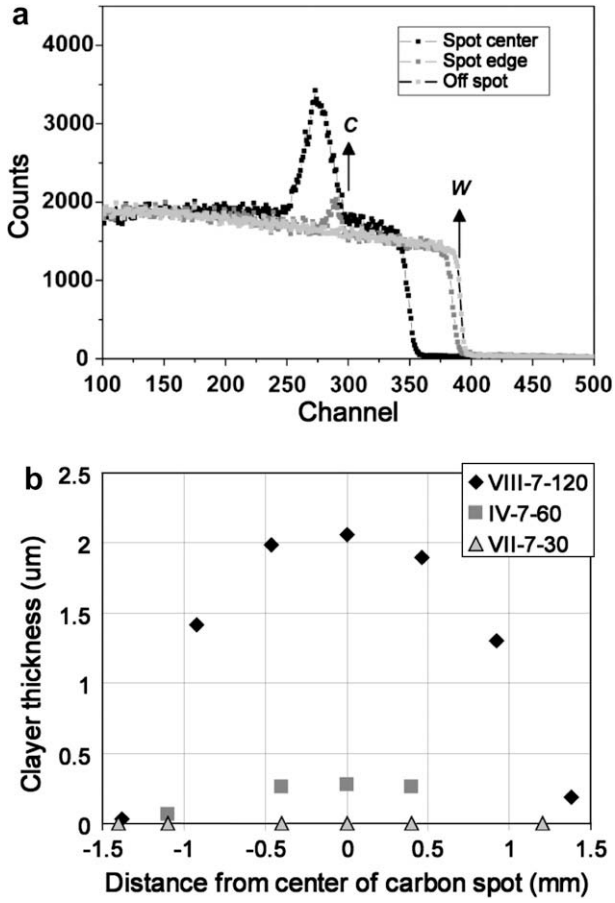


**Fig. 3.** (a) RBS spectra at various locations around carbon film on target VIII – 7–120 and (b) measured carbon film thicknesses by fitting $\mu$-beam proton RBS spectra.

Proton RBS results yield detailed measurements of C film thicknesses. The micro-beam was focussed to a beam spot diameter of ~5 μm and then raster scanned over an analysis spot of $170 \times 170$ μm$^2$ allowing for good spatial resolution across a carbon spot only ~2.7 mm in diameter (see Fig. 3b). The analysis of the carbon spot from W target VIII – 7–120 shows a well-defined carbon spot centered in the plasma column, indicating that C deposition is occurring in the regions of highest plasma density, electron temperature and surface temperature. This area also corresponds quite closely with the region where the CII emission line is strongest (Fig. 2b). Due to the local nature of the deposition (confined to the plasma column) and the close correspondence with the CII profile, it is inferred that the carbon film growth is driven and/or initiated by carbon ions in the plasma as opposed to the large neutral flux of carbon and hydrocarbons also striking the surface. Tungsten carbide formation may play a role in initiating the film growth since the highest temperatures, thus the best conditions for carbide formation, are at the center of the film growth location. However it should be noted that XPS scans showed no carbide formation at the edges of the carbon spot or in the regions outside the carbon spot. The deposited film is too thick for XPS to reach to the W–C interface in the center of the spot. However, it should be noted that, because these targets were exposed in the "as received" condition, it is possible that oxide layers on the surface (detected by XPS) may have impeded carbide formation.

The proton RBS spectra yield an areal concentration of carbon in the analysis spot and this, in combination with fitting of the shape of the spectra, yields C film thicknesses. In the spectra, the C peak can clearly be seen over the strong tungsten substrate signal due to the non-Rutherford cross section with proton scattering (Fig. 3a). The larger and broader C peaks correspond to thicker C films. As the C peak grows, the leading edge of the W component of the spectrum shifts to lower channels/energies, indicating there is no longer any W detectable on the surface. This is confirmed by XPS. The indications from the RBS spectra are that there is no detectable inter-material mixing between the C and W despite the high surface temperatures (~1200 K at the center of the spot) and thus highest C diffusion in W and greatest likelihood for tungsten carbide formation. Literature indicates that any intermixing would be under 50 nm in length scale for timescales of 120 s or less [11]. Since the depth resolution of the RBS is ~50 nm it is unlikely that any material mixing is detectable over these time or length scales.

The C film on target VIII – 7–120 was the thickest (Fig. 3b). The C film on target IV – 7–60 was also detectable with RBS although the maximum thickness was only ~300 nm. On target VII – 7–30 there was visible discolouration at the beam spot indicating the presence of a carbon deposit but there were too few counts for a reliable fit with the RBS. This indicates that there is a small amount of carbon on the beam spot of VII – 7–30 but the film thickness was less than the 50 nm depth resolution. However, XPS measurements did not detect any tungsten substrate at the location of the film, meaning the film was thicker than the probing depth of the XPS (~10 nm for a carbon-dominated surface). It is inferred the carbon film on VII – 7–30 is 10–50 nm in thickness. For targets VI – 7–10 and IX – 3–120 there was no visible discolouration of the surface and no carbon was detected with RBS either. The C film thicknesses are greatest at the center of the plasma column and decrease as the analysis point moves radially outwards (Fig. 3b), again coinciding

with the C-II signal. For target IX – 3–120 with the 3 sccm methane puff rate, it is not surprising there is no carbon film formation since Fig. 2a shows that there is minimal C-II signal for the 3 sccm puff rate and thus no carbon ions in the plasma to initiate or drive the C film growth. Sze et al. have also found a minimum required carbon concentration in the plasma to initiate carbon film growth on tungsten [2]. The minimum required carbon content for film growth found by Sze et al. was ~0.75 at.% at 850 K, however, this minimum decreased with increasing surface temperature. So it is possible for a lower minimum impurity level to be applicable in this study considering surface temperatures and plasma flux densities are higher. However, the minimum required carbon content value in combination with the fact that there was carbon film growth for 7 sccm puff rates and not for 3 sccm, indicates that the carbon content of the plasmas in this study are likely much closer to their calculated minimum values than the maximum values. For target VI – 7–10, the lack of detectable carbon indicates either some time delay before film growth can be initiated or a very thin film undetectable by RBS or by eye. XPS results were inconclusive on this target.

The effect of the carbon film on overall retention is determined with TDS. W targets were heated to 1273 K at a rate of ~1 K/s and the mass 4 ($D_2$) and mass 3 (HD) signals were monitored and calibrated to yield the total amount of retained deuterium. The peak structure changes dramatically between targets VIII – 7–120 and I – 0–120 (Fig. 4a). By comparing the desorption peak structure from VIII – 7–120 to the desorption peak structure from a pure graphite target desorption, it becomes evident that the desorption peaks in target VIII – 7–120 are dominated by the carbon film. Integrating the mass 4 and mass 3 signals the total D atoms retained in target VIII – 7–120 ($D_{retained} = 2.0 \times 10^{16}$ D atoms) is an order of magnitude greater than in target I – 0–120 ($D_{retained} = 1.6 \times 10^{15}$ D atoms) despite the carbon spot only covering ~5.7 $mm^2$ of the ~200 $mm^2$ exposed area of the tungsten target. The total retention scales roughly linearly with plasma exposure time ($\propto$ plasma fluence) as shown in Fig. 4b. This is expected for retention dominated by carbon co-deposition since this is an unsaturable retention mechanism. The zero offset in Fig. 4b is indicative of a minimum carbon film thickness before retention starts to become dominated by the co-deposition process. The total incident D fluence to the target can be determined through the integration of the bohm flux as determined by the Thomson scattering data (Fig. 1). Retained fractions ($D_{retained}/D_{incident}$) for targets with carbon films present is $(2 \pm 1) \times 10^{-6}$.

NRA was used to determine the retention locally, however, due to limited $^3$He ion energies, the maximum depth range for the NRA measurements was only ~3 μm. Measurement spots were taken at the center of the carbon spot, 2 mm off spot and 8 mm off spot. It is important to recognize that at these different locations the surface temperature and plasma ion fluxes are different as well as the carbon content of the plasma.

The NRA results clearly show an enhanced retention in the region of the carbon spot (Fig. 5). Retention in the region off the carbon spot is relatively unchanged supporting the results from TDS that the carbon film growth is responsible for the overall enhanced retention. Results are also consistent with the observation of no carbon film growth with a $CH_4$ injection rate of 3 sccm. The retention from 3 sccm injection rates are equivalent to those observed for exposure times of 10 and 30 s for 7 sccm injection rates where there is no or very little C deposition. The D retention for 2 mm off spot is slightly higher probably due to the lower local surface temperature while still being on the edge of the deposition region. The D retention for 8 mm off spot should not be influenced by carbon deposition and indicates the range in the natural scatter of retention data from target to target. This scatter has been discussed in more detail in [12]. For the 120 s exposure time the regions of C deposition (i.e. beam center and 2 mm off center) are roughly a factor of 10 higher than D retention in these regions for the 3 sccm injection rate with no C deposition, remaining consistent with the TDS results. NRA can produce depth profiles of local D concen-

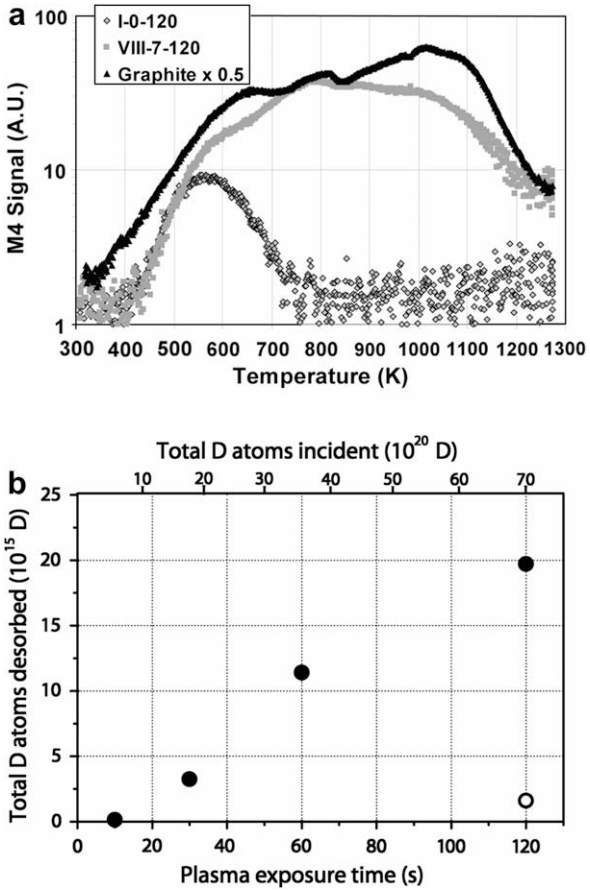


**Fig. 4.** (a) Mass 4 desorption spectrum from clean W, W + C, and pure C and (b) total D retention as a function of plasma exposure time and total incident D fluence; open symbol represents target I – 0–120 (no injected $CH_4$) and closed symbols represent targets VI – 7–10, VII – 7–30, IV – 7–60, and VIII – 7–120 (7 sccm $CH_4$ puffing rate).

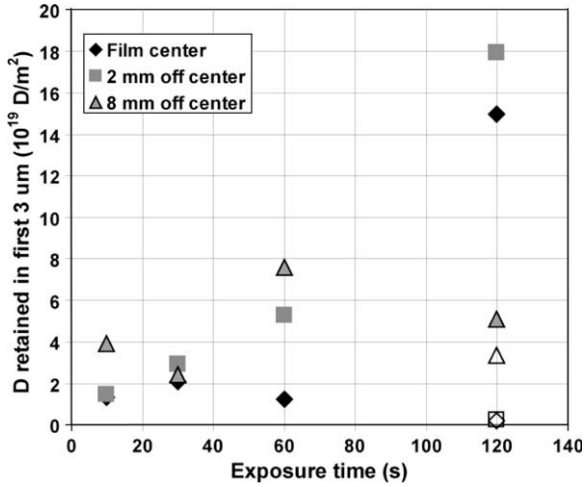


**Fig. 5.** Closed symbols are D retention as measured by NRA as a function of plasma exposure time for various radial positions and $CH_4$ puffing rate of 7 sccm. Open symbols represent target IX – 3–120 (3 sccm $CH_4$ puffing rate).

trations. The NRA parameters used for this study yield a depth profile in discrete steps of ~1 μm. Since the film thickness for target VIII – 7–120 is greater (~2 μm) than the discrete step size of the depth profile (~1 μm), it is possible to determine the local D concentration within the C film and thus determine the D/C ratio. For target VIII – 7–120, the D/C ratio of the film at the center location ($T_{surf} \sim 1200$ K) is 0.002 D/C. This low ratio is not unexpected for such high surface temperatures since it is well known that D/C ratios decrease with increasing surface temperatures [13] and can be < 0.01 D/C for temperatures above 1000 K [14].

## 4. Conclusions

The most obvious observation is the local deposition of carbon films on the tungsten substrates. Having the deposition be localized to the center of the plasma column indicates a confinement process was involved and in combination with the close correlation between carbon spot diameter and C-II signal profile, leads to the conclusion that the carbon film growth is initiated and/or driven by carbon ions in the plasma and not neutral atoms or molecules. This film growth can be rapid (highest measured deposition rate is 17.5 nm/s) in these high plasma density, high surface temperature scenarios, however the resulting films have low D/C ratios (0.002 D/C) due to the high surface temperatures during film growth. The rapid film growth under these conditions could lead to flaking and dust production from very thick deposits in a long pulse or steady-state device. It is also evident that net deposition of carbon is possible on a surface under high flux hydrogenic plasma bombardment even with low (<2%) carbon concentration in the plasma.

The growth of C films on the surface clearly enhances the hydrogenic retention of the tungsten targets. The enhanced retention is localized to the region of co-deposition and the regions where no film was formed have roughly equivalent retention rates to tungsten targets exposed to plasmas with no carbon seeding. Not only does the carbon film enhance retention, it dominates the retention properties of the tungsten targets. This indicates that, while pure tungsten targets have acceptable low hydrogenic retention rates for ITER, if a thick carbon (or any low-*Z*) film is co-deposited on the surface, the retention can become unfavorable, even if those films are deposited in a high density, high surface temperature scenario, such as the ITER divertor strikepoint regions.

## Acknowledgements

This work, supported by the European Communities under the contract of the Association EURATOM/FOM, was carried out within the framework of the European Fusion Programme with financial support from NWO. The views and opinions expressed herein do not necessarily reflect those of the European Commission.

## References

[1] J. Luthin, Ch. Linsmeier, J. Nucl. Mater. 290–293 (2001) 121.
[2] F.C. Sze, L. Chousal, R.P. Doerner, S. Luckhardt, J. Nucl. Mater. 266–269 (1999) 1212.
[3] Y. Ueda, T. Shimada, M. Nishikawa, Nucl. Fusion 44 (2004) 62.
[4] V.Kh. Alimov, J. Roth, R.A. Causey, D.A. Komarov, Ch. Linsmeier, A. Wiltner, F. Kost, S. Lindig, J. Nucl. Mater. 375 (2008) 192.
[5] W. Wang, V.Kh. Alimov, B.M.U. Scherzer, J. Roth, J. Nucl. Mater. 241–243 (1997) 1087.
[6] H. Atsumi, T. Tanabe, J. Nucl. Mater. 258–263 (1998) 896–901.
[7] G.J. van Rooij, V.P. Veremiyenko, W.J. Goedheer, et al., Appl. Phys. Lett. 90 (2007) 121501.
[8] H.J. van der Meiden, R.S. Al, et al., Rev. Sci. Instrum. 79 (2008) 013505.
[9] J. Westerhout et al., Appl. Phys. Lett. 95 (2009) 151501.
[10] W.A.J. Vijvers et al., Phys. Plasmas 15 (2008) 093507.
[11] K. Schmid, J. Roth, J. Nucl. Mater. 302 (2002) 96.
[12] G.M. Wright, A.W. Kleyn, E. Alves, et al., J. Nucl. Mater. 390–391 (2009) 610.
[13] V.Kh. Alimov, D.A. Komarov, J. Nucl. Mater. 313–316 (2003) 599.
[14] M. Mayer, V. Philipps, P. Wienhold, H.G. Esser, J. von Seggern, M. Rubel, J. Nucl. Mater. 290–293 (2001) 381.